ACS APPLIED MATERIALS & INTERFACES

Article

Near-Infrared Laser-Excited Nanoparticles to Eradicate Multidrug-Resistant Bacteria and Promote Wound Healing

Yue Qiao, Fei Ma, Chao Liu, Bo Zhou, Qiaolin Wei, Wanlin Li, Danni Zhong, Yangyang Li, and Min Zhou

ACS Appl. Mater. Interfaces, **Just Accepted Manuscript** • DOI: 10.1021/acsami.7b15251 • Publication Date (Web): 07 Dec 2017

ACS Publications

ACS Applied Materials & Interfaces is published by the American Chemical Society.
1155 Sixteenth Street N.W., Washington, DC 20036

Near-Infrared Laser-Excited Nanoparticles to Eradicate Multidrug-Resistant Bacteria and Promote Wound Healing

Yue Qiao,[†,‡] Fei Ma,[‡] Chao Liu,[§] Bo Zhou,[‡] Qiaolin Wei,[‡] Wanlin Li,[‡] Danni Zhong,[‡] Yangyang Li,[†] and Min Zhou*[,†,‡,∥,⊥]

[†]Department of Nuclear Medicine, The Second Affiliated Hospital of Zhejiang University, School of Medicine, Zhejiang University, Hangzhou 310009, China

[‡]Institute of Translational Medicine, Zhejiang University, Hangzhou, 310009, China

[§]Weifang Institute of Dermatology, Weifang 261057, China

[∥]Key Laboratory of early warning and intervention of malignant tumor (Ministry of Education), Zhejiang University, Hangzhou, 310009, China

[⊥]State Key Laboratory of Modern Optical Instrumentations, Zhejiang University, Hangzhou, 310058, China

*** Address correspondence to**

Email: zhoum@zju.edu.cn

Keywords: *Antibacterial, Multidrug-resistant bacteria, Triangular silver nanoparticles, Photothermal effects, Synergistic effect*

Abstract:

With the ever-growing threat of bacterial infections, especially for multidrug-resistant microbial infections, the development of highly effective treatment modalities to inhibit the infections is challenging. Although silver nanoparticles have been intensively applied as an antimicrobial agent for decades, the therapeutic efficacy towards multidrug-resistant bacteria is still unsatisfactory. Here, we show that near-infrared (NIR) laser-excited silver triangular nanoparticles (Tri-Ag) can efficiently kill Gram-negative *Escherichia coli* (*E. coli*) and Gram-positive *Staphylococcus aureus* (*S. aureus*) both *in vitro* and *in vivo*. Notably, multidrug-resistant bacterial clinical isolates, including methicillin-resistant *S. aureus* (MRSA) and extended spectrum beta-lactamase (ESBL) *E. coli* strain were significantly inhibited by the combined treatment of the Tri-Ag with NIR laser irradiation due to their synergistic antibacterial ability. Taking the advantage of its strong near-infrared absorbance, photothermal treatment is also conducted with Tri-Ag, achieving a remarkable synergistic antibacterial effect to inhibit various bacterial at a rather low concentration of this agent. Given the above advantages, the combination therapy of Tri-Ag with assistance of NIR laser may find potential applications to strengthen the antimicrobial arsenal for fighting bacterial infections.

1. Introduction

Given the increasing concern of bacterial infections, especially clinical-required antibiotic resistance, there is a growing need to develop new effective antibacterial treatments [1-4]. This is particularly true for multidrug-resistant bacteria-induced infections, which are difficult to cure because these organisms have the ability to develop rapidly antibiotic resistance [3,5]. For example, methicillin-resistant *S. aureus* (MRSA)-induced skin focal infections caused the dramatically increased incidence in recent years, presenting a serious threat to public health [6-8].

Recently, many antibacterial agents, such as antimicrobial peptides [9,10], polymers [11,12], quaternary ammonium salts [13], and inorganic nanoparticles (NPs) [14-20] were reported. Among them, inorganic NPs, including silver (Ag) [14,21-24], copper [25,26], gold [15,27], and other metal-based NPs [17-19,28-30], brought new opportunities for the development of safe and effective antibacterial therapeutics. Specifically, Ag NPs are becoming one of the most commonly applied agents to treat wounds, burns, and a variety of infectious diseases because of its outstanding antimicrobial properties against various microbials, including pathogenic bacteria, viruses, fungi, and other eukaryotic microorganisms [23,24]. The size, shape, and surface coating of Ag NPs were important factors for determining their antibacterial properties. It has been shown that different-sized Ag NPs exhibited different antibacterial effects [22]. For instance, Ag^+ ions dominated the bacterial toxicity of Ag NPs when the particle size is smaller than 10 nm,

while for larger particles, both the direct surface contact and ion release determined the antibacterial activity [22,31]. Friend *et al.* reported that triangular Ag NPs (Tri-Ag) demonstrated the highest antibacterial ability, compared with Ag nanospheres and Ag nanorods, due to their crystal structures whose (111) crystalline planes contain a mass of atoms. These special structures possibly disrupted the bacterial cell membrane permeability, disturbed its respiration functions when the NPs attach to the bacterial surface, and then showed more potent destructiveness in damaging the bacterial cell[32].

Owing to their unique optical properties, many inorganic NPs with NIR strong absorbance band, such as gold NPs [33,34], carbon nanomaterials [35,36], copper sulfide NPs [37-39], and palladium nanosheets [40,41], have been widely applied for photothermal therapy in cancer treatment. Combing NIR laser and strong light-absorbing nanomaterials, local high temperature was achieved surrounding the NPs and induced cancer cell death. The light energy can be converted to the thermal energy during the laser irradiation because of their strong NIR light absorption. By adjusting shape and size, the absorbance peak of silver NPs can be tuned to the NIR window. The tunable optical characteristics of these anisotropic silver NPs, especially for Tri-Ag, make it possible to treat the disease using laser-induced photothermal effects of these NPs. Likewise, Tri-Ag NPs with strong NIR absorbance also have great potential to elevate the temperature when they are exposed to NIR laser. The high local temperature could both destroy the surrounding bacterial membrane and accelerate Ag^+ release from the Ag NPs, which produce a synergistic effect to kill the bacterial. Therefore, Tri-Ag

combined with NIR laser for the antibacterial treatment may allow us to eliminate bacterial more effectively, even exterminate the multidrug-resistant microbials, and inhibit various bacteria-induced infections.

Here we present a NIR light-activatable photothermal therapeutic strategy that can not only eliminate Gram-negative *Escherichia coli* (*E. coli*) and Gram-positive *Staphylococcus aureus* (*S. aureus*) strains, but also can inhibit multidrug-resistant bacteria through their synergistic effect. We hypothesized that the synergistic effect could boost the disruption of the bacterial membrane and accelerate the release of Ag^+ with the stimulation of NIR laser irradiation. We synthesized Ag NPs and tuned their absorption to NIR region, which make it useful for photothermal treatment. The synergistic antibacterial effects were assessed in *E. coli* and *S. aureus* models, and were further evaluated by two multidrug-resistant bacterial strains (ESBL *E. coli* and MRSA). The possible mechanism of the combination treatment was carefully investigated through fluorescence imaging, scanning electron microscopy (SEM), and transmission electron microscopy (TEM). *In vivo* wound healing effects were tested by dressing in mouse skin defect model. Furthermore, the pilot *in vivo* toxicity study including blood and major organs histopathological examinations were evaluated.

2. RESULTS AND DISCUSSION

2.1 Preparation and characterization of Tri-Ag

Triangle silver nanoplates were synthesized by a facile one-step seedless synthetic method. One remarkable advantage of this seedless approach is that the surface plasmonic resonance (SPR) could be tuned to possess a wide spectral range from visible to the NIR region, through the change of the experimental parameters, such as the concentration of citrate. Precise synthesis of the Ag NPs to the NIR window is an important factor for the further biomedical application of the NPs through their photothermal effect. As the concentration of citrate decreased, the striking change of Ag NPs consequently resulted in the obvious red shift of SPR absorbance as shown in **Figure 1a**, and the color of the corresponding solutions (**Figure 1b**) changed from yellow to orange, green, purple, and then blue. As, we know, the optical properties are strongly dependent on the size and morphological feature of the Ag NPs. In the

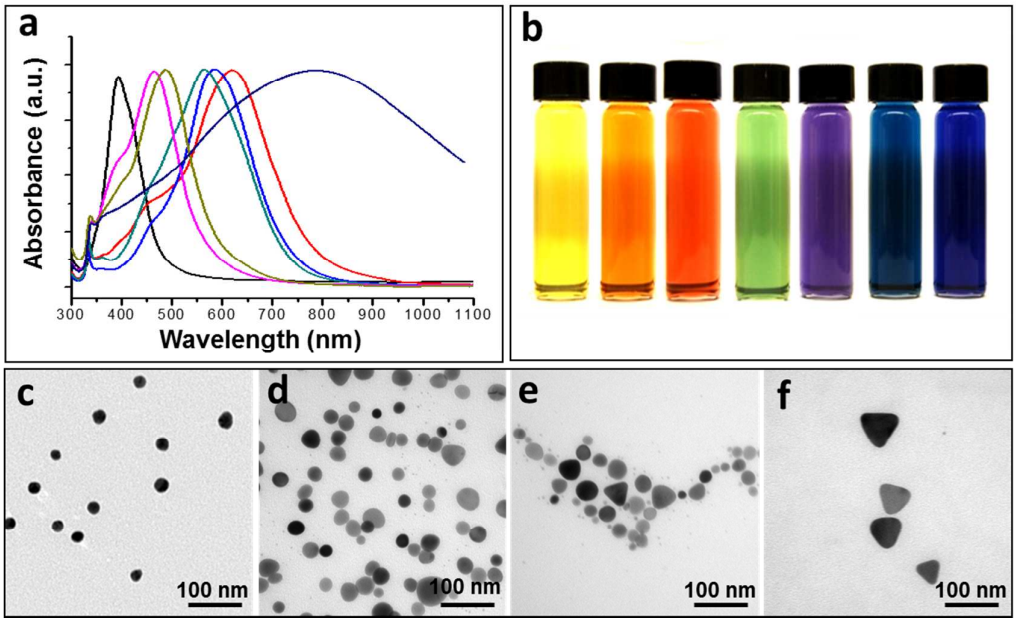

Figure 1. UV-vis absorption spectra (a) and the photograph (b) of the corresponding solutions of Ag NPs synthesized with different concentration of citrate. (c-f) The representative TEM images of Ag NPs underwent a progressive shape transition from nanospheres to triangular nanoplates.

representative TEM images (**Figure 1c-f**), the average particle size increased, and the resultant Ag NPs underwent a progressive shape transition from nanospheres to triangular nanoplates. **Figure 2a** showed the average diameter of the as-prepared triangular silver nanoplates (Tri-Ag), which was around 60 nm, and the thickness of the nanoplates is approximately 10 nm (the inset of **Figure 2a**). The hydrodynamic size of Tri-Ag is *c.a.* 62 nm, which was slightly larger than that from the TEM result (**Figure 2b**), may attribute to the coating of citrate. EDS results shown in **Figure 2c**

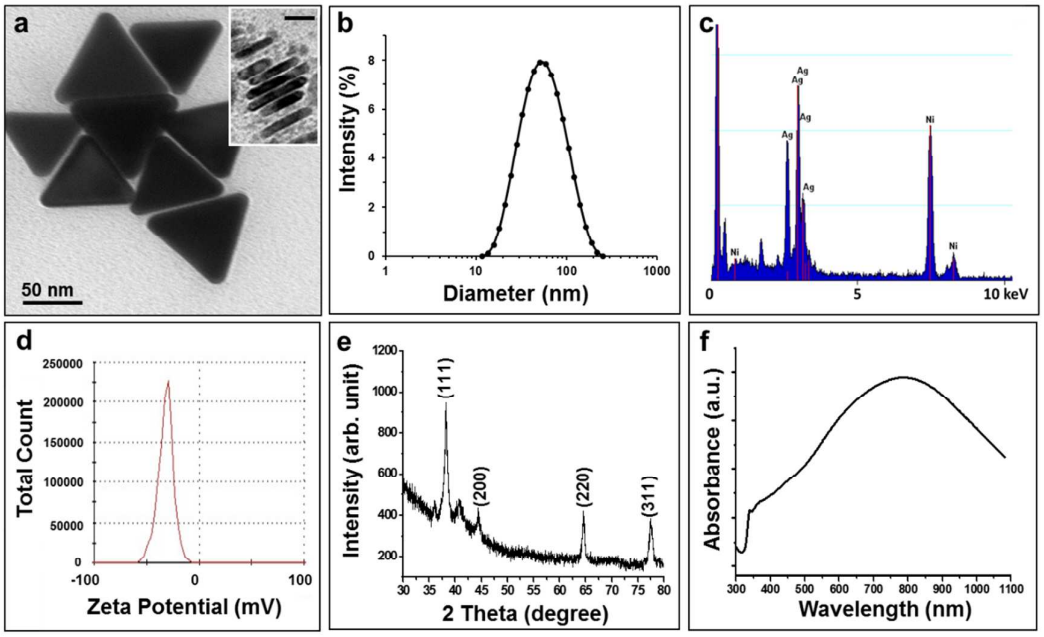

Figure 2. **Characterization of triangular Ag nanoparticles (Tri-Ag)**: a) TEM image of Tri-Ag, (inset: a TEM image of stacked Tri-Ag, the thickness of Tri-Ag determined from TEM image shows about 5 nm, bar: 20 nm); b) Size distribution Tri-Ag measured from dynamic light scatting; c) EDS spectrum of Tri-Ag indicating the element composition is silver; d) zeta potential of Tri-Ag showing the surface is negative; e) XRD of Tri-Ag shows its crystalline structure; f) UV-vis absorption spectrum of Tri-Ag in water showing a strong absorbance band in near-infrared region.

confirmed the presence of silver element in Tri-Ag (Ni element from the nickel grid for the TEM measurement). As shown in **Figure 2d**, the zeta potential of the Tri-Ag is -23.9 mV, indicating negative charges on the surface of NPs. The negative charge of Tri-Ag NP resulted from citrate during the synthesis could prevent the aggregation of the Tri-Ag in the aqueous solution due to strong electrostatic repulsion. Notably, Tri-Ag solution was stable for up to six months at room temperature, indicating their excellent stability. X-ray diffraction (XRD) analysis was applied to measure the crystalline structure of Tri-Ag (**Figure 2e**). The peaks obtained at 38.12°, 44.27°, 64.56°, and 77.34° were assigned to (111), (200), (220), and (311) plane, respectively. The remarkably strong peak at 38.12 from the (111) lattice plane implies that the NPs are made of pure silver and that their basal plane should be the (111) plane. Importantly, the optical absorption (**Figure 2f**) measured by UV-vis spectrometer demonstrated the Tri-Ag possessed strong absorption in NIR region, which was critically important for efficient NIR laser induced photothermal conversion.

2.2 Photothermal effect of Tri-Ag

We next systematically investigated the photothermal efficiency of the Tri-Ag owing to their strong NIR absorption. To confirm the capacity of Tri-Ag as a photothermal agent for PTT, temperature elevation tendency of Tri-Ag solution under an 808 nm NIR laser irradiation were measured. In **Figure 3**, the temperature of Tri-Ag sample raised quickly within 2 min and reached a plateau eventually. Moreover, the temperature rising rate increased with the laser power and NPs' concentration. For

instance, when the concentration of Tri-Ag was 25 μg/mL, the solution was heated up to ~88.2 °C within 6 min under laser exposure at 1.05 W/cm^2, while only 34.3 °C was reached with 0.3 W/cm^2 laser at the same Tri-Ag concentration. These results confirmed that the effective NIR laser-induced temperature elevation of Tri-Ag could be conveniently achieved and precisely tuned by adjusting the NPs' concentration as well as the laser energy. The photothermal conversion efficiency of Tri-Ag was calculated to be ~58.67 % (see Figure S1-2, in the Supporting Information). Importantly, more silver ions were released from Tri-Ag when the temperature increase (Figure S3, in the Supporting Information).

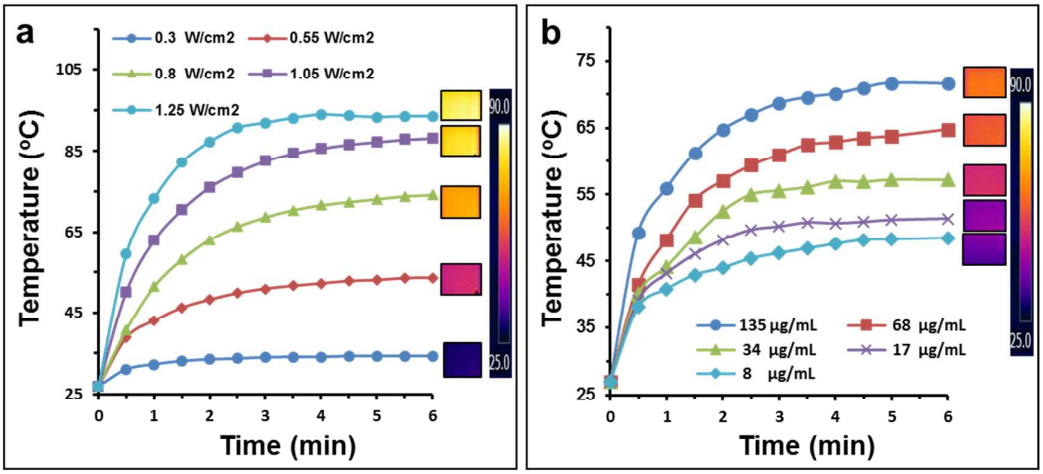

Figure 3. Photothermal effects of Tri-Ag aqueous solution: a) temperature changes of Tri-Ag solution at the concentration of 25 μg/mL with a series of power densities of 808 nm laser irradiation. Inset: temperature photographs of the Tri-Ag at the final temperature recorded by an infrared thermal camera; b) temperature changes of Tri-Ag at a series of concentration irradiated with a constant 808 nm laser power (1.0 W/cm^2). Inset: temperature photographs.

2.3 *In vitro* antibacterial activity of Tri-Ag

The antibacterial activities of Tri-Ag combined with NIR laser irradiation against both Gram-negative and Gram-positive sign were evaluated using *E. coli* and *S. aureus* (**Figure 4**) as model organisms, respectively. Spherical silver nanoparticles (Sph-Ag) were used as a control to compare their antibacterial effect with/without laser

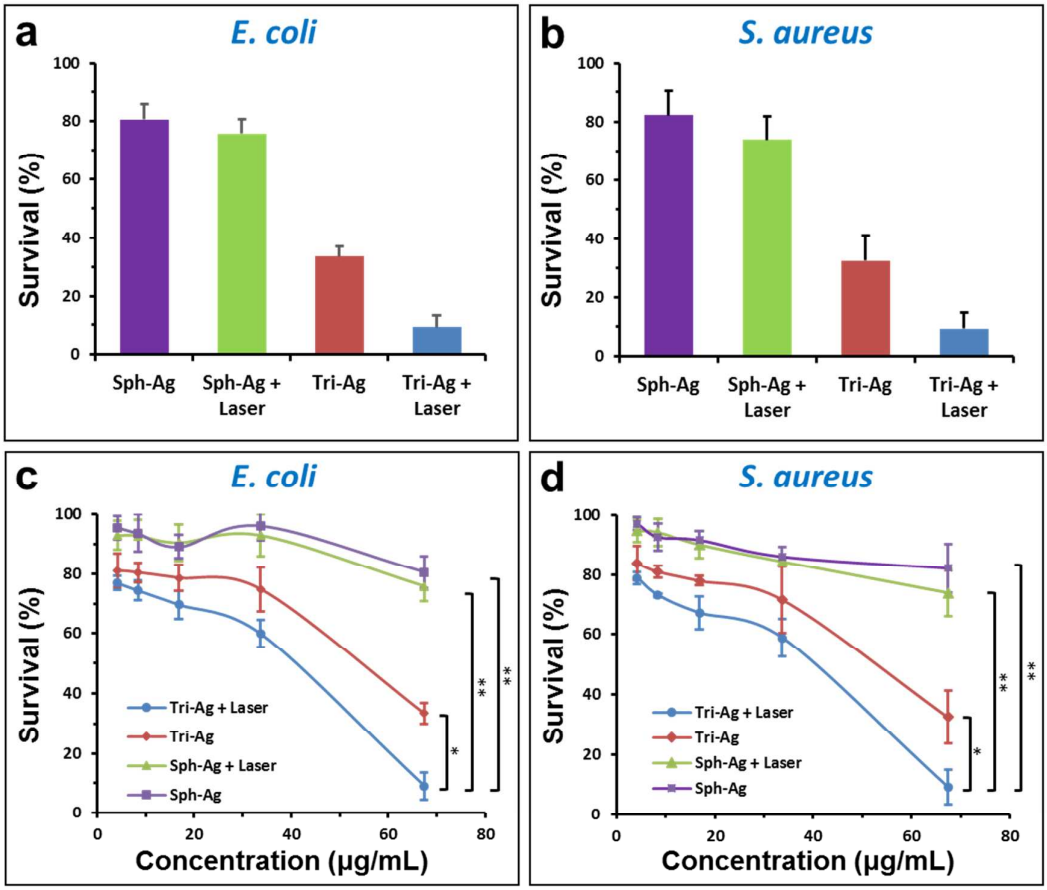

Figure 4. Antibacterial effect of Tri-Ag *in vitro*: survival rates of *E. coli* (a) and *S. aureus* (b) with various treatments at Ag concentration of 67.4 μg/mL. Power density was 1.0 W/cm^2 for 6 min. Survival rates of *E. coli* (c) and *S. aureus* (d) with various treatments at different Ag concentration. (*$p < 0.05$, **$p < 0.01$, ***$p < 0.001$)

irradiation. As compared to Sph-Ag (bacterial survival, 80.6% for *E. coli* and 82.1% for *S. aureus*), Sph-Ag groups even with the assistance of laser irradiation, the bacterial survival rates are still high (75.8% *E. coli* and 73.9% for *S. aureus*), when the Ag concentration is 67.4 μg/mL. This suggests that Sph-Ag or even plus NIR laser treatment cannot effectively kill the two bacterial strains. However, when the Tri-Ag was used for the treatment, the bacterial cells survival dramatically decreased to 33.5% (*E. coli*) and 32.5% (*S. aureus*), indicating their greater antibacterial ability. Surprisingly, more than 90% bacterial were eliminated by the Tri-Ag under the NIR laser irradiation (survival, 9.0% *E. coli* and 9.1% for *S. aureus*). Moreover, dose-dependent antibacterial ability was further by investigated. Tri-Ag plus laser treatment demonstrated the strongest antibacterial effect at all the same concentration conditions.

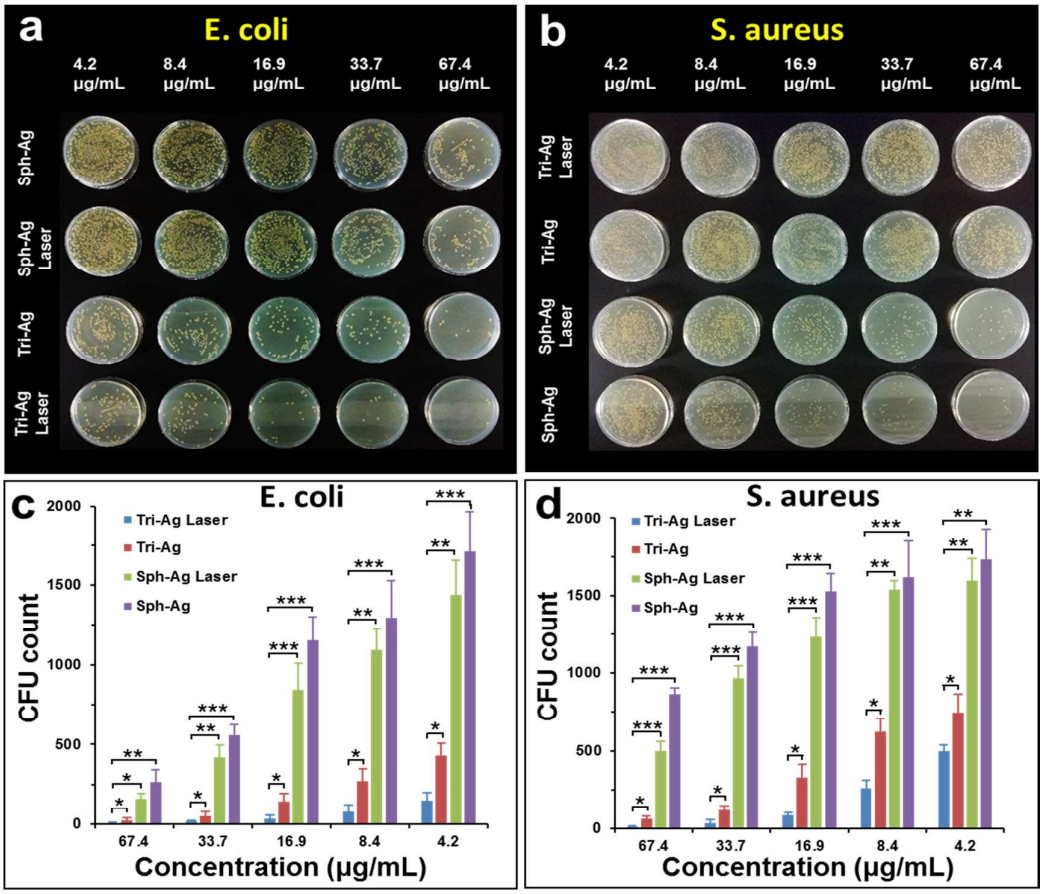

Figure 5. Photographs of bacterial colonies formed by *E. coli* (a) and *S. aureus* (b) with various treatments at different concentrations. Power density was 1.0 W/cm^2 for 6 min. The corresponding CFU count of *E. coli* (c) and *S. aureus* (d) with various treatments.

CFU plate counting method was also used to assess the antibacterial ability. The antibacterial results in all groups are in good agreement with the previous survival rates results. As shown in **Figure 5a,b**, Sph-Ag demonstrated a weak antibacterial effect even the concentration reached 67.4 μg/mL in two bacterial models, especially for *S. aureus*. The number of viable bacteria in the Sph-Ag plus laser exposure group was almost the same as the Sph-Ag group, indicating no synergistic effect for Sph-Ag and NIR laser irradiation. Tri-Ag with NIR laser irradiation showed better inhibition effects than all the other treatments, and nearly complete inhibition of bacterial growth

was observed at a total silver concentration of 4.2 μg/mL for both *E. coli* and 73.9% for and *S. aureus*. The quantitative analysis (**Figure 5c,d**) displayed that Tri-Ag plus laser treatment with various concentration (4.2, 8.4, 16.9, 33.7, and 67.4 μg/mL) reduced the number of colonies significantly, demonstrating their remarkable antibacterial ability.

2.4 In vitro assessment of antibacterial effects of drug-resistant bacteria

We also investigated the antibacterial activities of drug-resistant bacteria, including MRSA and EBSL *E. coli*. As shown in **Figure 6,** Tri-Ag combined with NIR laser irradiation showed the efficient antibacterial effects for both MRSA and ESBL *E. coli* bacteria. At high Ag concentration, whereas Sph-Ag group showed weak antibacterial effect (bacterial survival, 81.4% for MRSA and 81.8% for ESBL *E. coli*), Tri-Ag treatment demonstrated better effects (bacterial survival, 32.4% MRSA and 28.6% for ESBL *E. coli*). However, most of the bacteria (bacterial survival, 13.0% MRSA and 9.9%

for ESBL *E. coli*) were eradicated by the Tri-Ag plus laser treatment.

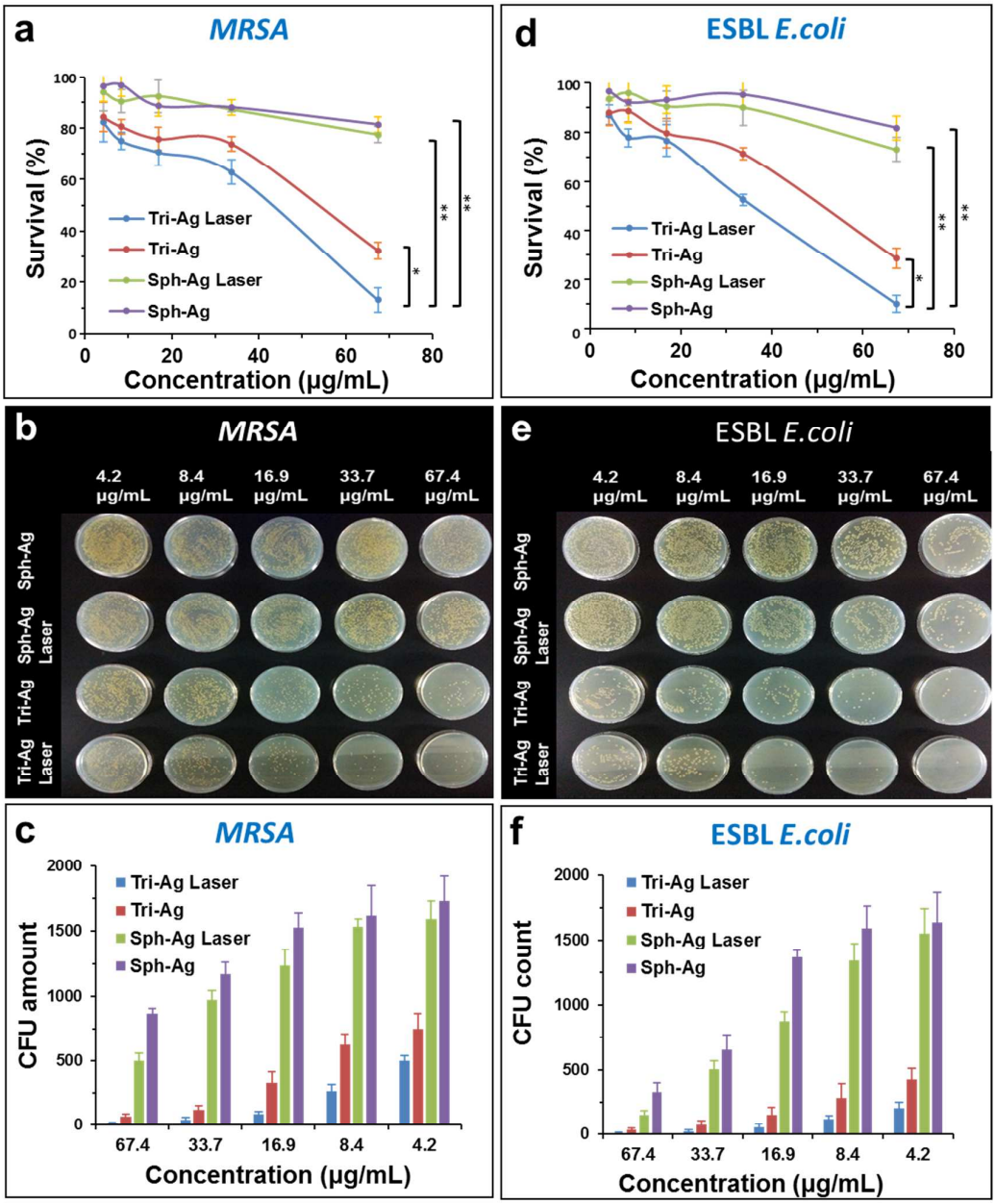

Figure 6. Anti-drug resistant bacterial effect of Tri-Ag: (a) *MRSA* growth survival; (b) Photographs of *MRSA* bacterial colonies formed on LB-agar plates; (c) CFU amount of MRSA bacteria. (d) ESBL *E. coli* growth survival; (e) Photographs of ESBL *E.coli* bacterial colonies formed on LB-agar plates; (f) CFU amount of ESBL *E.coli* bacteria.

Also, CFU colonies analysis demonstrated the similar results that most of the bacteria growth were significantly inhibited by Tri-Ag plus laser treatment. Therefore, the combination treatment is an excellent strategy to treat the drug resistant bacteria. We also made an antibacterial effect comparison of Tri-Ag Laser treatment and penicillin against ESBL *E. coli* and MRSA at the same concentration of 67.4 μg/mL and Tri-Ag Laser treatment had an obviously better treatment effect than penicillin both on ESBL *E. coli* and MRSA. The experimental procedure is roughly the same as above bacterial colonies forming experiment beside there was just one treatment concentration (Figure S7).

2.5 Cell integrity disruption of E. coli induced by Tri-Ag

The membrane integrity of *E. coli* on various treatments was analyzed using propidium iodide (PI) as a fluorescent nucleic acid dye, which could penetrate damaged membranes of bacteria to stain its DNA with red fluorescence. The fluorescence imaging result in **Figure 7a** showed that only very few *E. coli* could be stained by PI in the control group and the Sph-Ag plus laser group. It is obvious that some bacteria were stained red in the Tri-Ag group without laser irradiation. However, almost all the *E. coli* cells in the Tri-Ag plus laser treated group were stained red with PI, suggesting their synergistic antibacterial effect by disrupting cell wall/membrane integrity.

To further investigate the antibacterial mechanism of action of various treatments, TEM techniques were used to investigate the cell morphology on *E. coli* following various treatments. Indeed, a representative TEM image (**Figure 7b**) clearly showed that some Tri-Ag successfully penetrated into the cells. The morphology of the bacteria treated with Tri-Ag were significantly changed following the laser treatment, indicating the total cell death induced by the combination treatment.

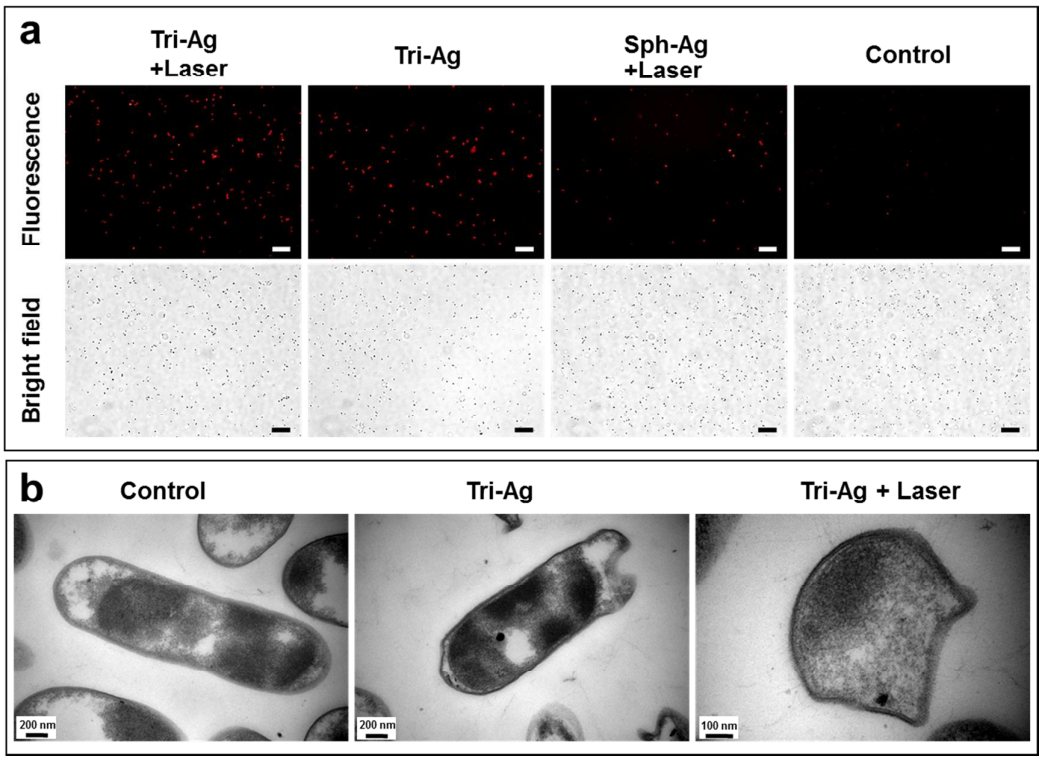

Figure 7. (a) Fluorescent and bright field photographs of E coli. stained by propidium iodide (PI) following various treatments, bar = 50 μm; (b) TEM images of *E. coli* treated with spherical Ag nanoparticles (Sph-Ag), Tri-Ag, and Tri-Ag plus laser, respectively.

SEM analysis also confirmed the membrane damage of the bacterial. In **Figure 8a**, no significant bacterial morphological changes were observed in Sph-Ag and Sph-Ag plus laser group, and slight damage to the cell membrane by Tri-Ag was observed,

membrane. However, the morphology of the bacterial cells treated by Tri-Ag plus laser was significantly changed. Much more noticeable holes were found on their cell walls, indicating major damage of the bacteria. In one representative SEM image (**Figure 8b**), a large number of plate-like nanostructures were clearly found on the surface of the bacteria. Also, the magnified SEM image (**Figure 8c**) demonstrated significant morphological changes including cell membrane broken and debris, clearly which representing serious damage to the bacterial walls that resulted in loss of cellular indicated that Tri-Ag only have weak disruption effect on the integrity of cell

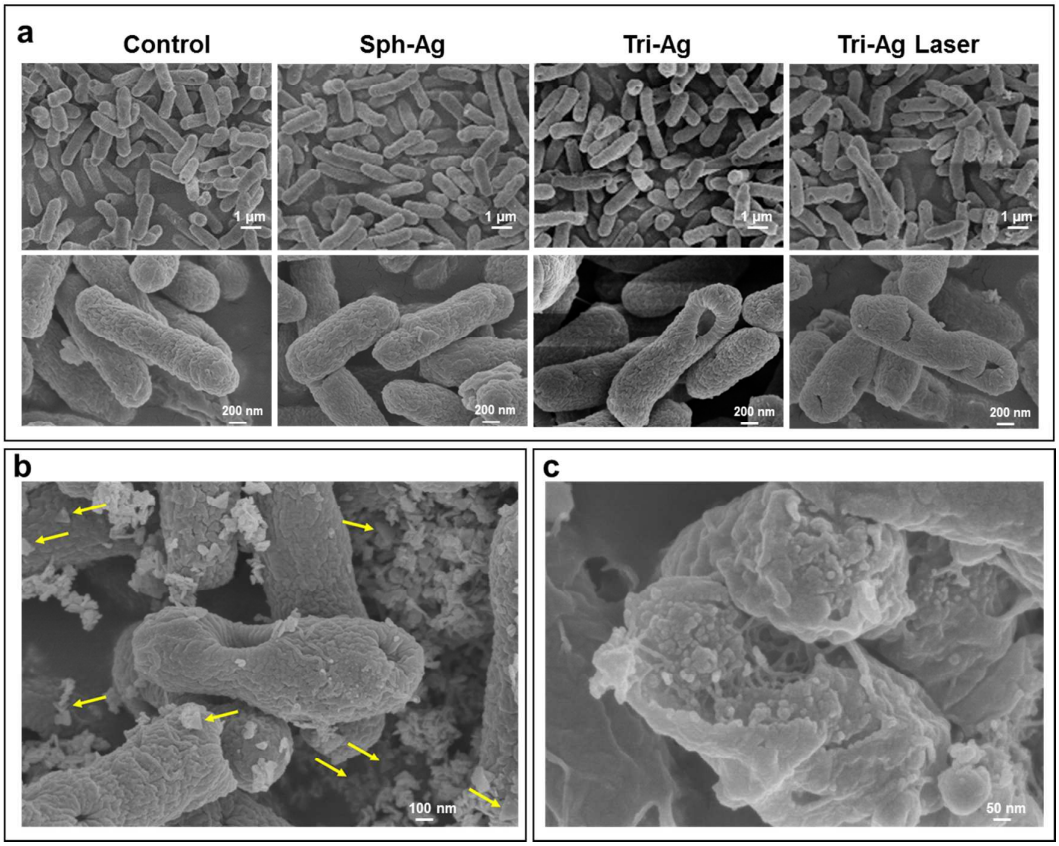

Figure 8. (a) SEM images of *E. coli* treated with spherical Ag nanoparticles (Sph-Ag), Tri-Ag, and Tri-Ag plus laser, respectively. The untreated group is used as the control 24 h after treatment. (b) a representative SEM image of Tri-Ag plus laser treated sample showing a large number of Tri-Ag on the surface of *E. coli*. 24 h after treatment. (c) a typical

SEM image of Tri-Ag plus laser treated *E. coli* demonstrating the destroyed bacterial structure 48 h after treatment

components when the treatment time increased to 48 h. The structures of the bacteria were totally destroyed, confirming the superior antibacterial function of Tri-Ag under NIR laser irradiation. The results above were also cooperated by the morphological studies of *E. coli* bacteria using SEM. Therefore, all the results revealed that the Tri-Ag was a superior agent with high effective synergistic antibacterial ability with the assistance of NIR laser irradiation.

Many reports investigated the reciprocity between the Ag NPs and the bacteria's cell membranes [32,42,43]. Cell membrane integrity can be destroyed and the structure was changed by the accumulation of Ag NPs on the bacteria's surface. The NPs can release Ag ions where the ions interact with sulfur related membrane protein, causing the cell membrane permeability changes. In this study, a large number of Tri-Ag onto the cell membrane were observed (**Figure 8**). The released silver ions could increase the cell membrane permeability by causing perforations and holes in bacterial membranes due to the direct interaction between the ions and the membrane proteins. Importantly, the ability to cause membrane damage is also beneficial when the cell surface temperature increase under the laser irradiation in the presence of Tri-Ag. Once this protective barrier of the bacteria breaks down, more Tri-Ag enter the internal of the bacteria. Then, the DNA molecule will lose its ability to replicate, thus affecting the bacterial viability, both for normal bacteria or multidrug-resistant bacteria. The Ag

ions also can induce enzyme inactivation of bacterial, when they interact with thiol groups of proteins. The deposition of proteins in cells was found when the Ag ions pass throught the cell wall. Tri-Ag demonstrated an obvious antimicrobial capacity compared with spherical Ag nanoparticles because of their high specific surface, which allows a larger area of contact with bacteria. When the bacteria were treated by heat (50 ^{o}C for 24 h). No obvious morphological changes were found after treatment. Therefore, enhanced antibacterial effects can be achieved owing to the synergistic effect.

2.6 *In vivo* wound healing Study

We also assessed *in vivo* healing ability in the wound-infecting bacterial skin of mice using the synergetic antibacterial strategy. We utilized female BALB/c mice with *MRSA* infected wound on their back as a model. After 10 min of irradiation, the temperature at the wound region of mice from silver NPs plus laser irradiation group increased strikingly to 49.9 ^{o}C. (**Figure 9a,b**). Conversely, the wound regions of the mice in the Sph-Ag plus laser group treated by laser exhibited very limited increase (37.8 ^{o}C after 10 min of laser treatment) in temperature, indicating that NIR laser at such a lower power density by itself could not change the wound temperature significantly. We photographed the traumas, measure the wound surface area every 2 days, and carried out histological evaluations of the mouse dermal wound tissues on day 8 to examine the wound healing inflammation and any potential side effects. **Figure 9c** showed representative macroscopic photos and closure of wounds with various treatments at

different time points. Compared with other groups, the deep black scars appeared in Tri-Ag plus laser treatment groups at the second day. On day 12, the wounds for all treatment groups became smaller and even disappeared for synergistic Tri-Ag plus laser were still observed for other groups. The edema and ulceration were observed except that the synergistic group even after 8 days. Considering the whole healing process, this treatment can accelerate wound closure and decrease the possibility of infection and death. Conversely, compared to the wound treated with Sph-Ag plus laser or Tri-Ag, the wounds were smaller than the control but still much larger than the wound of the mice in Tri-Ag plus laser group. For the histological analysis, the control group possessed mass inflammatory cells, suggesting that the wound recovery was not complete. The Sph-Ag plus laser group and Tri-Ag group also showed fewer inflammatory cells. However, the wounds of the synergistic group demonstrate almost entire epidermis structure and did not find obvious inflammation or infection, indicating complete healing effect. Moreover, the antibacterial effect *in vivo* was further assessed by determining the surface area in wound region (**Figure 9d**). Compared with other NIR group whereas the wound boundary and incomplete dermal groups, the surface area of the wounds demonstrates that treatment with synergetic Tri-Ag plus laser group decrease rapidly, resulting in the surface area decreased to 11.96%, whereas control, laser only, and Tri-Ag group can only be decreased to 78.07%, 64.94%, and 53.84%, respectively. Therefore, the synergistic Tri-Ag plus laser antibacterial treatment can effectively kill bacteria, promote the scar generation to protect wound tissue, and accelerate the wound closure. Since reactive oxygen species (ROS) play a

critical role in wound healing, we investigate the ROS effects of the different treatment. **Figure S6** demonstrated strong ROS effects of Tri-Ag plus laser illumination and Tri-Ag treatments, whereas the Tri-Ag plus laser displayed highest ROS effect.

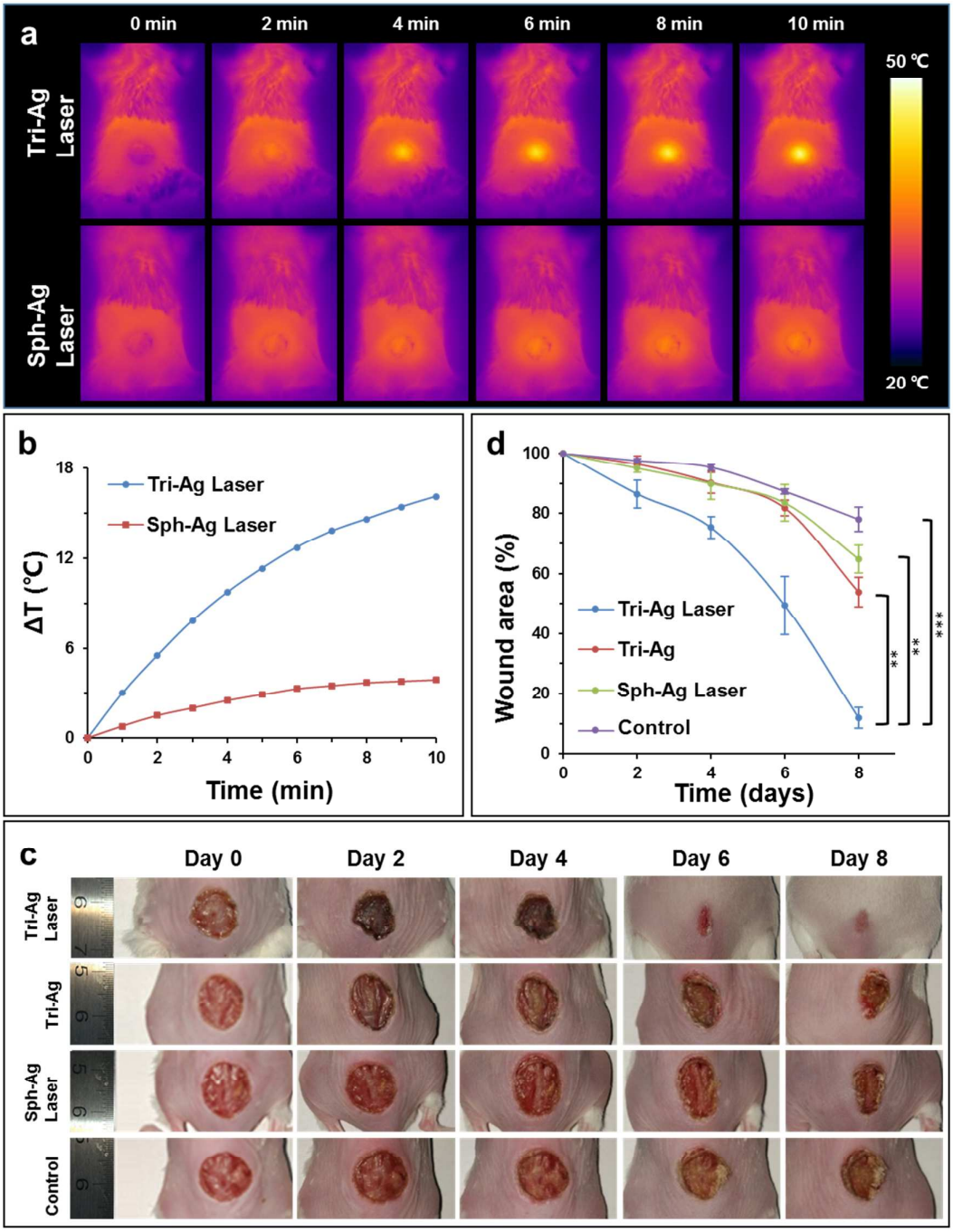

Figure 9. *In vivo* experiments to evaluate the Tri-Ag plus laser technique: (a) Thermal infrared image of temperature evolution on dosed mice upon NIR laser irradiation; (b) Temperature evolution profile of dosed mice upon NIR laser irradiation; (c) Wound photographs for effects of treatment of MRSA infected wound of mice; (d) Wound area evolution rate of mice.

Moreover, we further evaluated the wound healing progress by hematoxylin and

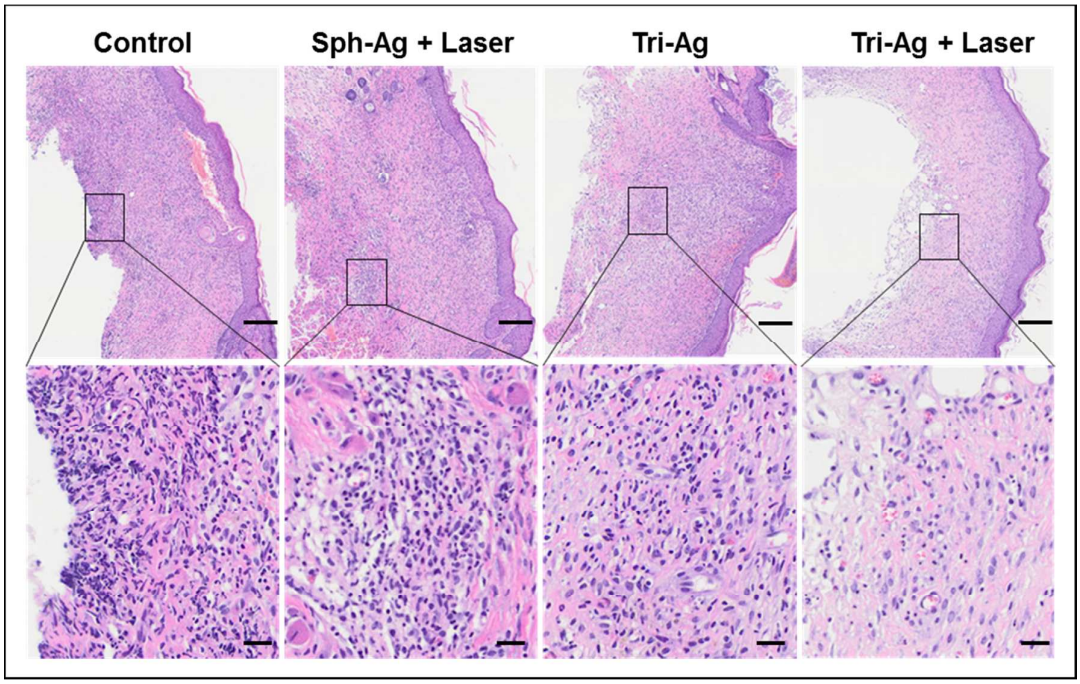

Figure 10. Histological observation of mice tissues after treatments: H&E staining of the mice dermal wound for pathological observation at day 8 after treatment, bar: up = 200 μm; bottom = 50 μm.

eosin stained sections (H&E staining). In **Figure 10**, a large amount of inflammatory cells and fragmentary epidermal layer appeared on the wound after treatments with the control, Sph-Ag, and Tri-Ag groups, while the intact epidermal layer as well as less inflammatory cells emerged on the wound treated with Tri-Ag plus laser treatment.

Thus, it can be concluded that Tri-Ag plus laser treatment exhibited the best antibacterial effect and wound healing effect among various treatments.

2.7 Pilot toxicity study *in vivo*

Although the *in vivo* antibacterial study only involved epidermal treatments by Tri-Ag or Sph-Ag, we still evaluated the potential toxicity for the safety concerns. The histology analysis of the major organs (heart, liver, spleen, kidney, and lung) (**Figure 11**) demonstrated normal tissue structures without any obvious inflammatory lesions or organ damage after the treatment. No appreciable signs of toxic behaviors and neither noticeable change of body weight nor mortality was seen in all four groups (**Figure 12a**). The biosafety of the treatments was also assessed by blood biochemistry and hematology analysis after *in vivo* antibacterial study. No significant difference in blood biochemistry and hematology parameters were observed, indicating normal liver and kidney functions (**Figure 12 b-l**). The preliminary studies confirmed the Tri-Ag plus laser treatment's biosafety *in vivo*, indicating that the treatment can act as an excellent antibacterial agent to inhibit bacteria growth and accelerate the wound healing with minimal toxicity at the tested dose. However, more systematic investigations, such as immune-compatibility and long-term toxicity studies, are still needed before the future clinical translation.

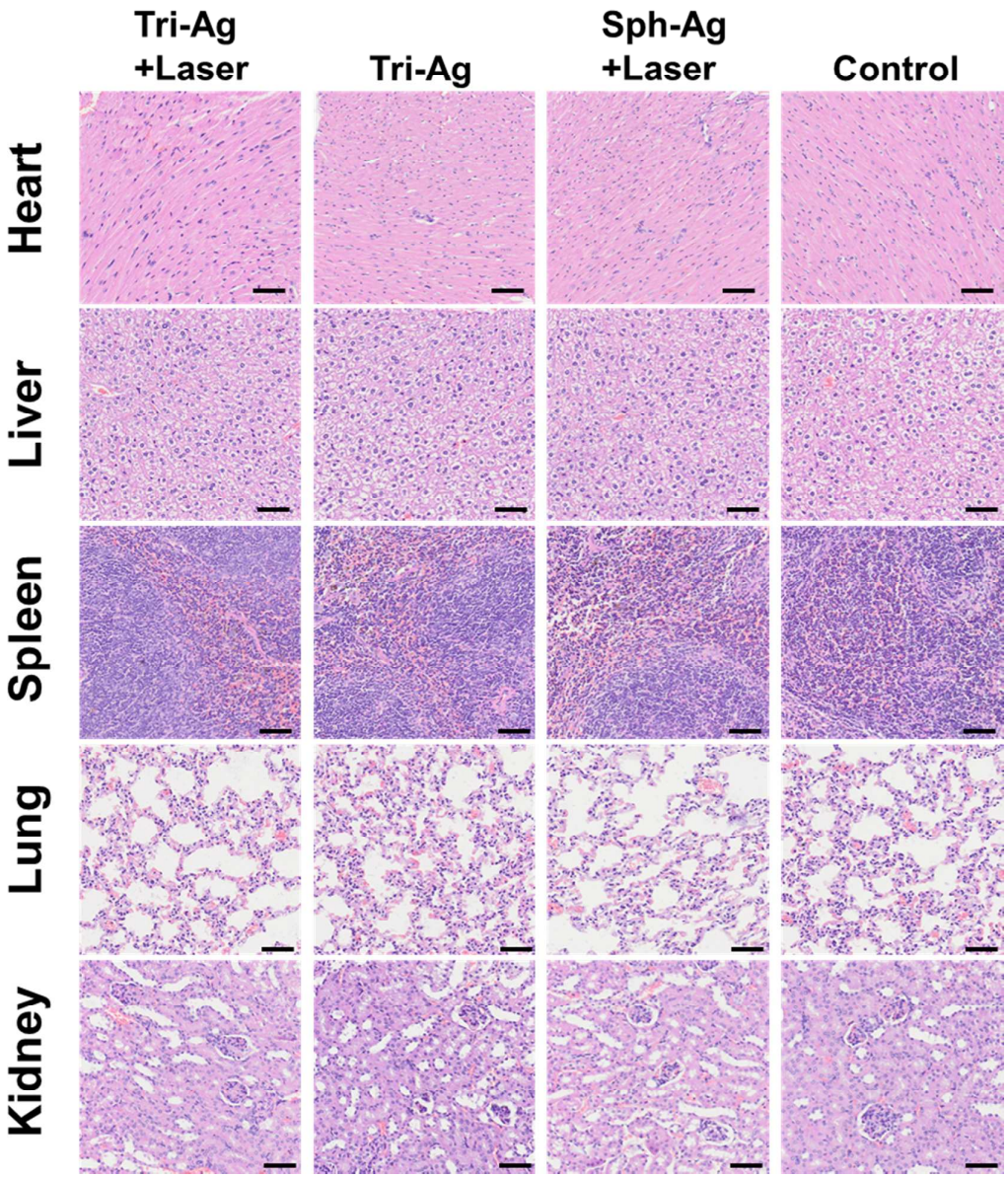

Figure 11. Preliminary toxicity analysis in major organs: H&E staining of the major organs of mice heart, liver, spleen, lung, and kidney for toxicological observation, bar = 50 μm.

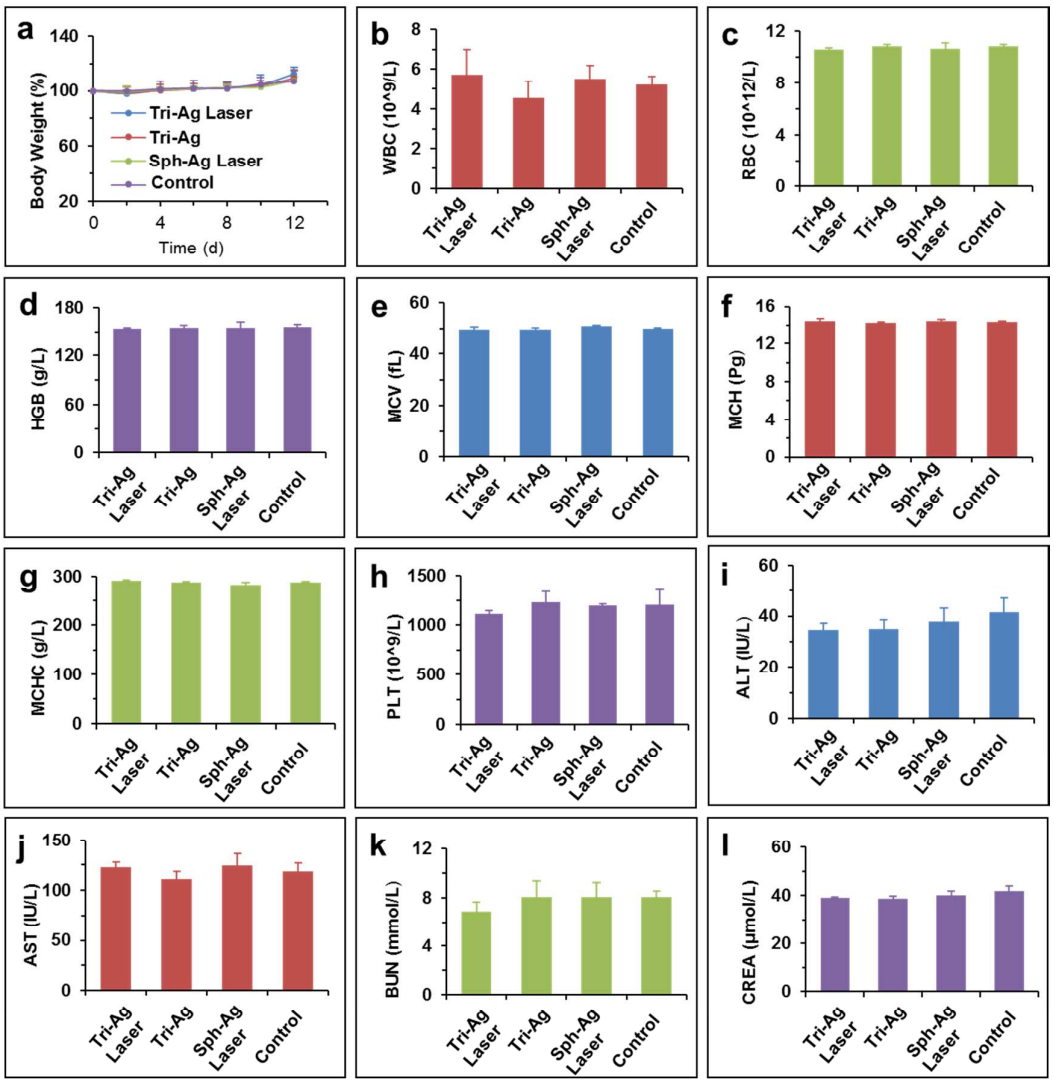

Figure 12. The influence of mice healthy: (a) body weight, (b-l) blood biochemistry and hematology survey. WBC, white blood cells; RBC, red blood cells; HGB, haemoglobin; MCV, mean cell volume; MCH, mean corpuscular haemoglobin; MCHC, mean corpuscular haemoglobin concentration; PLT, blood platelet; ALT, alanine transferase; AST, aspartate transferase; BUN, blood urea nitrogen; CREA, Creatitine.

3. Conclusions

In summary, we have successfully developed a synergistic antibacterial system based on a simple combination between Tri-Ag and NIR laser irradiation. We showed that the combination treatment can eradicate both Gram-positive *E. coli* and Gram-negative *S. aureus* bacteria. More importantly, our data demonstrated that Tri-Ag has an antimicrobial synergistic effect against multidrug-resistant bacterial in both ESBL *E. coli* and MRSA strains when it was used in combination with NIR laser. Enhanced morphological changes in the bacterial membrane induced by Tri-Ag with laser irradiation may contribute to the bacterial death after the combination treatment. Importantly, the wound infected by multidrug-resistant bacteria in the mouse model could be recovered effectively after the synergetic antibacterial strategy was applied, which does not induce any obvious toxicity *in vivo* in our preliminary safety evaluation. This work provided a simple, effective way to inhibit the bacterial infections and has great potential on fighting against multidrug-resistant bacteria-induced diseases in the clinical research and translation infection.

4. Experimental Section

4.1 Materials

Silver nitrate, sodium citrate dihydrate, hydrogen peroxide solution (30 wt. %), and sodium borohydride were purchased from Sigma-Aldrich. *E. coli* (ATCC 25922), *S. aureus* (ATCC 6538), ESBL *E. coli*, and MRSA were obtained from the American type

culture collection (Rockville, MD).

4.2 Synthesis of Tri-Ag and Sph-Ag

The synthesis of Tri-Ag was carried out by a one-step chemical approach. A 100 mL aqueous solution containing of sodium citrate (10 mL, 70 mM), silver nitrate (100 μL, 50 mM), and hydrogen peroxide solution (1 mL, 30 wt.%) was stirred vigorously at room temperature under dark condition. After introducing of sodium borohydride (1 mL, 0.1 M), the solution turned to yellow immediately, then to blue at 20 min, indicating the formation of Tri-Ag. Various morphologies of silver NPs was tuned by changing the concentration of sodium citrate. The similar approach was used for the synthesis of silver nanospheres. No hydrogen peroxide was used, but keeping the same procedures during the preparation.

4.3 Characterization

The morphologies of Ag NPs were measured by using a Tecai 20 transmission electron microscopy (TEM, FEI, USA). The absorptions of Ag NPs were recorded on a UV−vis spectrometer (SHIMADZU UV-2600, Japan). Hydrodynamic size and zeta potential measurements was determined at room temperature by a Malvern Zetasizer Nano ZS90. X-ray diffraction (XRD) patterns were characterized by a Rigaku X-ray diffractometer. The NIR laser used for treatment was operated at 808 nm (Infrared Diode Laser system, Changchun CNI, China). The temperature elevation mediated by Tri-Ag was tested with 808 nm NIR laser exposure at various power densities. The

Sph-Ag was as control. The corresponding temperature was recorded by means of a thermal camera (Flir A300, USA).

4.4 In vitro antibacterial activity

Gram-negative *E. coli*, Gram-positive *S. aureus*, EBSL *E. coli*, and MRSA were used for the assessment of the antibacterial ability of Tri-Ag. Different concentration (4.2 μg/mL, 8.4 μg/mL, 16.9 μg/mL, 33.7 μg/mL, 67.4 μg/mL) of Tri-Ag or Sph-Ag**,** were added to the lysogeny broth (LB) medium containing the bacteria cells. The solution was illuminated with/without 808 nm laser (10 min, 1.3 W/cm^2). Twenty-four hours after incubation, the bacterial solution was taken into 96-well plates, and the optical density at 600 nm (OD_{600}) was measured to estimate the bacteria concentration using a multi-mode microplate reader (SpectraMax M5, USA). Thereafter the bacterial suspension of each group was diluted 10^6 folds, and 100 μL of the dilutions were spread onto LB plates to grow for 24 h at 37 °C. The colonies were calculated at 72 h after treatment, and each assay was carried out in triplicates.

4.5 Morphological characterization of bacteria.

Fluorescent-based cell dead method also determined the bacterial death assay. 1.5 mL of the bacterial cells (5×10^7 CFU/mL) was collected and rinsed with PBS (pH 7.4). The suspension was treated with Tri-Ag or Sph-Ag at the same concentration of 67.4 μg/mL and illuminated 808 nm laser (10 min, 1.3 W/cm^2) or not. After the mixture cultured for 1 h, propidium iodide (50 μL, 30 μM) fluorescent dyes was introduced to

the cells and incubated for further 15 min. All samples were observed under an inverted fluorescence microscope (Leica DMI 4000B, Germany).

For SEM measurement, the bacterial suspension (5.0×10^7 CFU/mL) was collected and washed three times, and then were cultured with Tri-Ag (67.4 μg/mL) for 1 h. Ten min after laser exposure (1.3 W/cm^2), all the suspensions were centrifuged (5000 rpm) and washed with PBS. The bacteria cells were fixed on the glass with 2.5% glutaraldehyde solution, washed with PBS, dehydrated with ethanol, and dried under vacuum. The samples were coated with platinum and then imaged by a scanning electron microscope (SEM; Hitachi SU-8010, Japan). For TEM measurement, the Tri-Ag Laser group bacteria was also pelleted and washed by PBS, and then fixed, and characterized by a TEM (FEI Tecnai 20, USA).

4.6 *In vivo* antibacterial study

All animal experiments were approved by the Institutional Animal Care and Use Committee of Zhejiang University. Female BALB/c mice were obtained from Shanghai Bioscience Co., Ltd. All mice were individually raised in cages under standardized temperature. The animals were anesthetized by 10% chloral hydrate, and then one wound was prepared on the backbone of mouse with a surgical scalpel, over a surface of circle (diameter of 7 mm). The mice (n = 3) were divided into four groups: Tri-Ag laser group, Tri-Ag group, Sph-Ag laser group, and untreated control group. 50 μL of the bacterial mixture (suspension of equal volume and concentration of *MRSA* bacteria, 2.0×10^7 CFU/mL) was used to infect the tissue of all the mice. After 24 h, the pus was

observed on the infected wound and 50 μL of 67.4 μg/mL. Tri-Ag or Sph-Ag was smeared on the wounds except the untreated group which were treated with 50 μL of 0.9% NaCl solution instead. The wounds in mice from Tri-Ag laser group and Sph-Ag laser group were treated by laser (10 min, 1.3 W/cm^2). The temperature changes on mice wound area were monitored by a thermal imaging system during the entire therapy course. The size of the wounds was measured every 2 days. After 8 days, wound recovery was observed and the tissue samples were obtained for pathological histology analysis.

4.7 Pilot toxicity study

Toxicity experiments were carried out with mice *in vivo* study. After in vivo wound healing experiments, all mice were euthanized by CO_2 exposure. Then, blood samples were cardiac punctured for hematologic and clinical chemistry analysis. The major organs were removed for toxicology analysis.

4.8 Statistical analysis

Differences in antibacterial data were analyzed using the two-tailed Student's t test. Differences between groups were considered statistically significant at $p < 0.05$.

AUTHOR INFORMATION

Corresponding Author

* Email: zhoum@zju.edu.cn

Conflict of Interest: The authors declare no competing financial interest.

AUTHOR CONTRIBUTIONS

M.Z. acted as principal investigator, conceived and designed the experiments with assistance from Y.Q., F.M., and C.L.. Y.Q. and B.Z. synthesized the nanoparticles. B.Z., Q.W. and W.L. characterized the nanoparticles. Y.Q., F.M., and D.Z. performed the in vitro antibacterial analysis and mechanism experiments. Y.Q. and F.M. performed the in vivo wound healing studies. Y.Q., D.Z., and C.L. carried out the toxicity experiment. Y.L. performed the ROS analysis. M.Z., Q.Y., and C.L. wrote the paper.

ACKNOWLEDGMENT

This work was supported by the National Key Research and Development Program of China (2016YFA0100900), National Natural Science Foundation of China (No.

81671748), the Project of Chinese Thousand Youth Talents, and China Postdoctoral Science Foundation (2017M620243).

REFERENCES

(1) Jones, K. E.; Patel, N. G.; Levy, M. A.; Storeygard, A.; Balk, D.; Gittleman, J. L.; Daszak, P. Global trends in emerging infectious diseases. *Nature* **2008**, *451*, 990-U994.

(2) Magiorakos, A. P.; Srinivasan, A.; Carey, R. B.; Carmeli, Y.; Falagas, M. E.; Giske, C. G.; Harbarth, S.; Hindler, J. F.; Kahlmeter, G.; Olsson-Liljequist, B.; Paterson, D. L.; Rice, L. B.; Stelling, J.; Struelens, M. J.; Vatopoulos, A.; Weber, J. T.; Monnet, D.

L. Multidrug-resistant, extensively drug-resistant and pandrug-resistant bacteria: an international expert proposal for interim standard definitions for acquired resistance. *Clin. Microbiol. Infect.* **2012**, *18*, 268-281.

(3) Brown, E. D.; Wright, G. D. Antibacterial drug discovery in the resistance era. *Nature* **2016**, *529*, 336-343.

(4) Burnham, C. D.; Leeds, J.; Nordmann, P.; O'Grady, J.; Patel, J. Diagnosing antimicrobial resistance. *Nat. Rev. Microbiol* **2017**, 15, 697-703

(5) Howard, S. J.; Hopwood, S.; Davies, S. C. Antimicrobial Resistance: A Global Challenge. *Sci. Transl. Med.* **2014**, *6*, 236ed210.

(6) Koeser, C. U.; Holden, M. T. G.; Ellington, M. J.; Cartwright, E. J. P.; Brown, N. M.; Ogilvy-Stuart, A. L.; Hsu, L. Y.; Chewapreecha, C.; Croucher, N. J.; Harris, S. R.; Sanders, M.; Enright, M. C.; Dougan, G.; Bentley, S. D.; Parkhill, J.; Fraser, L. J.; Betley, J. R.; Schulz-Trieglaff, O. B.; Smith, G. P.; Peacock, S. J. Rapid Whole-Genome Sequencing for Investigation of a Neonatal MRSA Outbreak. *New Engl. J. Med.* **2012**, *366*, 2267-2275.

(7) Laxminarayan, R.; Duse, A.; Wattal, C.; Zaidi, A. K. M.; Wertheim, H. F. L.; Sumpradit, N.; Vlieghe, E.; Hara, G. L.; Gould, I. M.; Goossens, H.; Greko, C.; So, A. D.; Bigdeli, M.; Tomson, G.; Woodhouse, W.; Ombaka, E.; Peralta, A. Q.; Qamar, F. N.; Mir, F.; Kariuki, S.; Bhutta, Z. A.; Coates, A.; Bergstrom, R.; Wright, G. D.; Brown, E. D.; Cars, O. Antibiotic resistance-the need for global solutions. *Lancet Infect. Dis.* **2013**, *13*, 1057-1098.

(8) Lindsay, J. A. Hospital-associated MRSA and antibiotic resistance—What have we learned from genomics? *Int. J. Med. Microbiol.* **2013**, *303*, 318-323.

(9) Choudhury, H. G.; Tong, Z.; Mathavan, I.; Li, Y.; Iwata, S.; Zirah, S.; Rebuffat, S.; van Veen, H. W.; Beis, K. Structure of an antibacterial peptide ATP-binding cassette transporter in a novel outward occluded state. *Proc. Natl. Acad. Sci. USA* **2014**, *111*, 9145-9150.

(10) Fernandez-Lopez, S.; Kim, H. S.; Choi, E. C.; Delgado, M.; Granja, J. R.; Khasanov, A.; Kraehenbuehl, K.; Long, G.; Weinberger, D. A.; Wilcoxen, K. M.; Ghadiri, M. R. Antibacterial agents based on the cyclic D,L-alpha-peptide architecture. *Nature* **2001**, *412*, 452-455.

(11) Magennis, E. P.; Fernandez-Trillo, F.; Sui, C.; Spain, S. G.; Bradshaw, D. J.; Churchley, D.; Mantovani, G.; Winzer, K.; Alexander, C. Bacteria-instructed synthesis of polymers for self-selective microbial binding and labelling. *Nat. Mater.* **2014**, *13*, 748-755.

(12) Cheng, Z. P.; Zhu, X. L.; Shi, Z. L.; Neoh, K. G.; Kang, E. T. Polymer microspheres with permanent antibacterial surface from surface-initiated atom transfer radical polymerization. *Ind. Eng. Chem. Res.* **2005**, *44*, 7098-7104.

(13) Jia, Z. S.; Shen, D. F.; Xu, W. L. Synthesis and antibacterial activities of quaternary ammonium salt of chitosan. *Carbohydr. Res.* **2001**, *333*, 1-6.

(14) Morones, J. R.; Elechiguerra, J. L.; Camacho, A.; Holt, K.; Kouri, J. B.; Ramirez, J. T.; Yacaman, M. J. The bactericidal effect of silver nanoparticles. *Nanotechnology* **2005**, *16*, 2346-2353.

(15) Zhao, Y.; Tian, Y.; Cui, Y.; Liu, W.; Ma, W.; Jiang, X. Small Molecule-Capped Gold Nanoparticles as Potent Antibacterial Agents That Target Gram-Negative Bacteria. *J. Am. Chem. Soc.* **2010**, *132*, 12349-12356.

(16) Allahverdiyev, A. M.; Abamor, E. S.; Bagirova, M.; Rafailovich, M. Antimicrobial effects of TiO_2 and Ag_2O nanoparticles against drug-resistant bacteria and leishmania parasites. *Future Microbiol.* **2011**, *6*, 933-940.

(17) Natalio, F.; André, R.; Hartog, A. F.; Stoll, B.; Jochum, K. P.; Wever, R.; Tremel, W. Vanadium pentoxide nanoparticles mimic vanadium haloperoxidases and thwart biofilm formation. *Nat Nanotechnol.* **2012**, *7*, 530-535.

(18) Das, D.; Nath, B. C.; Phukon, P.; Dolui, S. K. Synthesis and evaluation of antioxidant and antibacterial behavior of CuO nanoparticles. *Colloids Surf. B* **2013**, *101*, 430-433.

(19) Talebian, N.; Amininezhad, S. M.; Doudi, M. Controllable synthesis of ZnO nanoparticles and their morphology-dependent antibacterial and optical properties. *J. Photochem. Photobiol. B* **2013**, *120*, 66-73.

(20) Chatterjee, A. K.; Chakraborty, R.; Basu, T. Mechanism of antibacterial activity of copper nanoparticles. *Nanotechnology* **2014**, *25*, 135101.

(21) Kim, J. S.; Kuk, E.; Yu, K. N.; Kim, J.-H.; Park, S. J.; Lee, H. J.; Kim, S. H.; Park, Y. K.; Park, Y. H.; Hwang, C.-Y.; Kim, Y.-K.; Lee, Y.-S.; Jeong, D. H.; Cho, M.-H. Antimicrobial effects of silver nanoparticles. *Nanomed. Nanotechnol. Biol. Med.* **2007**, *3*, 95-101.

(22) Rai, M.; Yadav, A.; Gade, A. Silver nanoparticles as a new generation of antimicrobials. *Biotechnol. Adv.* **2009**, *27*, 76-83.

(23) Franci, G.; Falanga, A.; Galdiero, S.; Palomba, L.; Rai, M.; Morelli, G.; Galdiero, M. Silver Nanoparticles as Potential Antibacterial Agents. *Molecules* **2015**, *20*, 8856-8874.

(24) Ping, Y.; Hu, X.; Yao, Q.; Hu, Q.; Amini, S.; Miserez, A.; Tang, G. Engineering bioinspired bacteria-adhesive clay nanoparticles with a membrane-disruptive property for the treatment of Helicobacter pylori infection. *Nanoscale* **2016**, 8, 16486-16498.

(25) Maillard, J. Y.; Hartemann, P. Silver as an antimicrobial: facts and gaps in knowledge. *Crit. Rev. Microbiol.* **2013**, 39, 373-383.

(26) Ruparelia, J. P.; Chatteriee, A. K.; Duttagupta, S. P.; Mukherji, S. Strain specificity in antimicrobial activity of silver and copper nanoparticles. *Acta Biomater.* **2008**, *4*, 707-716.

(27) Li, X.; Robinson, S. M.; Gupta, A.; Saha, K.; Jiang, Z.; Moyano, D. F.; Sahar, A.; Riley, M. A.; Rotello, V. M. Functional Gold Nanoparticles as Potent Antimicrobial Agents against Multi-Drug-Resistant Bacteria. *ACS Nano* **2014**, *8*, 10682-10686.

(28) Huang, W.-C.; Tsai, P.-J.; Chen, Y.-C. Multifunctional Fe_3O_4@Au Nanoeggs as Photothermal Agents for Selective Killing of Nosocomial and Antibiotic-Resistant Bacteria. *Small* **2009**, *5*, 51-56.

(29) Hu, W.; Peng, C.; Luo, W.; Lv, M.; Li, X.; Li, D.; Huang, Q.; Fan, C. Graphene-Based Antibacterial Paper. *ACS Nano* **2010**, *4*, 4317-4323.

(30) Courtney, C. M.; Goodman, S. M.; McDaniel, J. A.; Madinger, N. E.; Chatterjee, A.; Nagpal, P. Photoexcited quantum dots for killing multidrug-resistant bacteria. *Nat. Mater.* **2016**, *15*, 529-534.

(31) Avalos, A.; Haza, A. I.; Mateo, D.; Morales, P. Interactions of manufactured silver nanoparticles of different sizes with normal human dermal fibroblasts. *Int. Wound J.* **2016**, *13*, 101-109.

(32) Pal, S.; Tak, Y. K.; Song, J. M. Does the antibacterial activity of silver nanoparticles depend on the shape of the nanoparticle? A study of the Gram-negative bacterium Escherichia coli. *Appl. Environ. Microbiol.* **2007**, *73*, 1712-1720.

(33) Gobin, A. M.; Lee, M. H.; Halas, N. J.; James, W. D.; Drezek, R. A.; West, J. L. Near-infrared resonant nanoshells for combined optical imaging and photothermal cancer therapy. *Nano Lett.* **2007**, *7*, 1929-1934.

(34) Chen, J. Y.; Glaus, C.; Laforest, R.; Zhang, Q.; Yang, M. X.; Gidding, M.; Welch, M. J.; Xia, Y. N. Gold nanocages as photothermal transducers for cancer treatment. *Small* **2010**, *6*, 811-817.

(35) Antaris, A. L.; Robinson, J. T.; Yaghi, O. K.; Hong, G.; Diao, S.; Luong, R.; Dai, H. Ultra-low doses of chirality sorted (6,5) carbon nanotubes for simultaneous tumor imaging and photothermal therapy. *ACS Nano* **2013**, *7*, 3644-3652.

(36) Yang, K.; Zhang, S. A.; Zhang, G. X.; Sun, X. M.; Lee, S. T.; Liu, Z. A. Graphene in mice: ultrahigh in vivo tumor uptake and efficient photothermal therapy. *Nano Lett.* **2010**, *10*, 3318-3323.

(37) Zhou, M.; Song, S. L.; Zhao, J.; Tian, M.; Li, C. Theranostic CuS nanoparticles targeting folate receptors for PET image-guided photothermal therapy. *J. Mater. Chem. B* **2015**, *3*, 8939-8948.

(38) Zhou, M.; Li, J.; Liang, S.; Sood, A. K.; Liang, D.; Li, C. CuS Nanodots with Ultrahigh Efficient Renal Clearance for Positron Emission Tomography Imaging and Image-Guided Photothermal Therapy. *ACS Nano* **2015**, *9*, 7085-7096.

(39) Zhou, M.; Zhang, R.; Huang, M.; Lu, W.; Song, S.; Melancon, M. P.; Tian, M.; Liang, D.; Li, C. A chelator-free multifunctional [^{64}Cu]CuS nanoparticle platform for simultaneous micro-PET/CT imaging and photothermal ablation therapy. *J. Am. Chem. Soc.* **2010**, *132*, 15351-15358.

(40) Tang, S.; Chen, M.; Zheng, N. Sub-10-nm Pd Nanosheets with Renal Clearance for Efficient Near-Infrared Photothermal Cancer Therapy. *Small* **2014**, *10*, 3139-3144.

(41) Huang, X. Q.; Tang, S. H.; Mu, X. L.; Dai, Y.; Chen, G. X.; Zhou, Z. Y.; Ruan, F. X.; Yang, Z. L.; Zheng, N. F. Freestanding palladium nanosheets with plasmonic and catalytic properties. *Nat. Nanotechnol.* **2011**, *6*, 28-32.

(42) Jung, W. K.; Koo, H. C.; Kim, K. W.; Shin, S.; Kim, S. H.; Park, Y. H. Antibacterial activity and mechanism of action of the silver ion in Staphylococcus aureus and Escherichia coli. *Appl. Environ. Microbiol.* **2008**, *74*, 2171-2178.

(43) Morones-Ramirez, J. R.; Winkler, J. A.; Spina, C. S.; Collins, J. J. Silver Enhances Antibiotic Activity Against Gram-Negative Bacteria. *Sci. Transl. Med.* **2013**, *5*, 11.

Table of Contents Graphic